

Joint Spectrum Mapping of Polarization Entanglement in Spontaneous Parametric Down-conversion

Hou Shun Poh, Chune Yang Lum, Ivan Marcikic, Antía Lamas-Linares, and Christian Kurtsiefer
Department of Physics, National University of Singapore, Singapore, 117542
(Dated: September 23, 2018)

Polarization-entangled photon pairs can be efficiently prepared into pure Bell states with a high fidelity via type-II spontaneous parametric down-conversion (SPDC) of narrow-band pump light. However, the use of femtosecond pump pulses to generate multi-photon states with precise timing often requires spectral filtering to maintain a high quality of polarization entanglement. This typically reduces the efficiency of photon pair collection. We experimentally map the polarization correlations of photon pairs from such a source over a range of down-converted wavelengths with a high spectral resolution and find strong polarization correlations everywhere. A spectrally dependent imbalance between contributions from the two possible decay paths of SPDC is identified as the reason for a reduction in entanglement quality observed with femtosecond pump pulses. Our spectral measurements allow to predict the polarization correlations for arbitrary filter profiles when the frequency degree of freedom of the photon pairs is ignored.

I. INTRODUCTION

Spontaneous parametric down-conversion (SPDC) is the basis for the most common method of generating entangled photons for use in quantum information protocols [1]. Typically, this process is used in two different regimes distinguished by the properties of the pump source. Initial experiments on SPDC [2, 3, 4] and applications for quantum key distribution [5] make use of a continuous pump light (cw), where entangled states can be prepared with high brightness and fidelity in various degrees of freedom [6, 7].

The other regime covers experiments in which photon pairs need to exhibit tight localization in time [8, 9], or when more than one pair should be simultaneously generated [10]. In such cases, short optical pulses with a coherence time compatible with that of the down-converted photons (on the order of few 100 fs) have to be used as a pump [11]. The short pulse duration implies a wide distribution of pump frequencies. In combination with the dispersion relations of the nonlinear optical material this leads to entanglement of the polarization degree of freedom with the spectral properties of the down-converted photons [12]. For the purpose of generating pure entangled states in only one variable, this is generally detrimental, manifesting itself as a degree of mixedness when only the polarization is considered (with the exception of the work reported in [13]). Thus there is a strong interest in improving the quality and brightness of pulsed sources of polarization-entangled photons. While there are several proposals and demonstrations [14, 15, 16, 17, 18] based on spectral and temporal engineering to address the separation of spectral degrees of freedom, none of them has been widely adopted.

This paper presents an experimental study of the influence of the spectral degree of freedom on polarization entanglement for traditional type-II SPDC sources in a femtosecond pulsed regime, e.g. as those used in experiments on teleportation [8] and entanglement swapping [19]. In the following section, we briefly discuss the basic process

of SPDC using short pump pulses. In Section III, we outline an experimental set-up to simultaneously study the spectral and polarization correlations, which we present in Section IV as mappings of the joint spectral properties of the down-converted photons. Section V covers the degree of polarization entanglement in different areas of the joint spectrum and in Section VI the effects of different spectral filtering on the purity of an observed state are analyzed. We briefly summarize in Section VII.

II. ENTANGLEMENT AND SPECTRAL DISTINGUISHABILITY

As in early experiments to entangle photon pairs in atomic cascade decays [20], the process of SPDC is able to generate polarization-entangled photons because two different decay paths result in two-photon states which are indistinguishable apart from their polarization degree of freedom. This can be seen from the simplest description of SPDC which is formulated in terms of three plane wave optical modes. The input corresponds to a narrow-band pump mode with a well defined wave vector \vec{k}_p , and output modes with wave vectors \vec{k}_s , \vec{k}_i may be populated via down-conversion if phase matching conditions and energy conservation are fulfilled [3]:

$$\begin{aligned}\vec{k}_p &= \vec{k}_s + \vec{k}_i \\ \omega_p &= \omega_s + \omega_i\end{aligned}\quad (1)$$

In some birefringent materials, these conditions can be satisfied in two different ways, producing either an horizontally/vertically (H_1V_2) or a V_1H_2 polarized pair [4]. If the two processes are truly indistinguishable, a photon pair may be observed in a pure state:

$$|\Psi\rangle = \frac{1}{\sqrt{2}} (|H\rangle_1|V\rangle_2 + e^{i\delta}|V\rangle_1|H\rangle_2) \quad (2)$$

For cw pumped down-conversion, this simple argument is enough to account for the presence of polarization

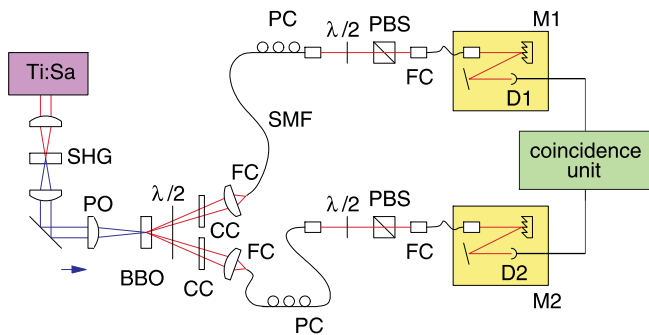


FIG. 1: Schematic of the spontaneous parametric down-conversion (SPDC) set-up. A femtosecond-pumped SPDC process generates photon pairs in single mode optical fibers which pass through polarization filters and subsequent grating monochromators.

entanglement and properties such as the bandwidth of down-converted photons [4, 21]. However, in a pulsed pump regime, the short duration of the pump imposes a Fourier limited spread of the input energy. Together with the broader phase matching conditions due to the difference in the dispersion relations for the ordinary and extraordinary waves in birefringent materials, this gives rise to spectral signatures which distinguish the two down-conversion processes. Leakage of polarization information into degrees of freedom which are not normally monitored results in mixedness of the polarization state of the photon pair. This effect of the spectral information can be observed by jointly measuring the spectral and polarization correlations between the down-conversion modes.

III. EXPERIMENTAL SET-UP

In order to perform spectrally resolved polarization correlation measurements on the down-converted photons, we implemented a photon pair source using traditional type-II phase matching, followed by polarization analyzers and grating monochromators to resolve the different spectral components for both photons (Fig. 1).

The output of a Ti:Sapphire (Ti:Sa) laser (central wavelength $\bar{\lambda}_c = 780$ nm, pulse duration ≈ 150 fs, repetition rate 76 MHz, average power 1.1 W) is frequency doubled (SHG) to produce optical pulses at $\bar{\lambda}_p = 390$ nm. This light (average power 400 mW) passes through pump optics (PO) to correct for the astigmatism and to focus the beam down to a waist of $80 \mu\text{m}$. At the focus, a 2 mm thick BBO crystal cut for collinear type-II phase matching ($\theta = 43.6^\circ$, $\phi = 30.0^\circ$) serves as the non-linear medium for down-conversion. The crystal is oriented such that the wavelength-degenerate decay paths emerge with distinct directions. A half-wave plate ($\lambda/2$) and a pair of compensation crystals (CC) take care of temporal and transversal walk-off [4].

The spatial modes of the down-converted photons, de-

finied by single mode optical fibers (SMF), are matched to the pump mode to optimize the collection [21]. In type-II SPDC, each down-converted pair consists of one ordinary and one extraordinarily polarized photon, and our set-up is aligned such that ordinary corresponds to vertical (V), while extraordinary corresponds to horizontal (H) polarization after compensation. A pair of polarization controllers (PC) is used to ensure that the SMF do not affect the polarization of the collected photons. To arrive at an approximate singlet Bell state $|\Psi\rangle$, the free phase δ between the two decay possibilities in the polarization state Eq. (2) is adjusted to $\delta = \pi$ by tilting the CC.

The polarization analysis in each arm is performed by a combination of another half-wave plate ($\lambda/2$) and a polarizing beam splitter (PBS), allowing projections onto any arbitrary linear polarization. The transmitted photons are transferred into grating monochromators on each arm (M1, M2) with 0.3 nm (FWHM) resolution and then detected with passively quenched Silicon avalanche photodiodes (D1, D2). Output of the two detectors is sent into a coincidence unit with a coincidence window shorter than the repetition period of the pump laser.

With the photons from the SMF sent directly into D1 and D2, bypassing the monochromators, a coincidence rate of 48000s^{-1} is observed. The total coupling and detection efficiency extracted from the ratio of pair coincidences to single detector events on one side is 11%.

Polarization entanglement of photon pairs prepared in such a set-up is often tested by probing the polarization correlations in a complementary basis; for Bell states $|\Psi^\pm\rangle$, strong polarization correlations are expected for observing photons in $\pm 45^\circ$ linear polarizations. We will quote this correlation as a visibility V_{45} in the coincidence rates obtained by fixing one of the analyzers to a 45° orientation and rotating the direction of the other analyzer.

With interference filters of 5 nm bandwidth (FWHM) centered at 780 nm replacing the monochromators, we observe a visibility $V_{45} = 81.7 \pm 0.3\%$, whereas the visibility in the H/V basis as the natural basis of the type-II down-conversion process reaches $V_{HV} = 94.0 \pm 0.4\%$. This indicates a relatively low entanglement quality or a mixedness of the photon pair state.

Before analyzing the joint spectral properties we note that the down-conversion modes are individually (i.e., not observed in coincidence with the other photon in the pair) characterized by central wavelengths of $\bar{\lambda}_1 = 779.8$ nm and $\bar{\lambda}_2 = 779.3$ nm. Corresponding widths of the approximately Gaussian wavelength distributions for extraordinary and ordinary polarization are $\Delta\lambda_H \approx 8.3$ nm (FWHM) and $\Delta\lambda_V \approx 9.9$ nm (FWHM), respectively.

IV. SPECTRAL CORRELATIONS

To investigate the relation between the spectral distribution and the polarization correlations, the monochromators M1, M2 were used in conjunction with the polarization analyzer. In the experimental runs, we fix the polarization analyzer orientations α_1, α_2 and record a two-dimensional map of coincidence events for a fixed integration time at each wavelength pair (λ_1, λ_2) .

First, we consider the joint spectra of photon pairs for each of the two decay paths individually. Therefore, analyzers were fixed to the natural basis of the conversion crystal, selecting either H_1V_2 or V_1H_2 decays. The corresponding joint spectra acquired with a resolution of 0.5 nm are shown as density plots in Fig. 2. The integration time for each wavelength pair in this map was 22.5 seconds. For both polarization combinations, we observe approximately two-dimensional Gaussian distributions, which are almost aligned along one of the diagonals as suggested by the energy conservation for the down-conversion process. Contrary to a case with a narrow-band cw pump [22], the distribution is not restricted to a single line corresponding to a fixed energy sum $E_p = hc(\lambda_1^{-1} + \lambda_2^{-1})$. However, the covariance between the two wavelengths λ_1, λ_2 is not completely lost. This is mostly attributed to the larger bandwidth of the pump due to its short duration. We further note that the two joint spectra for H_1V_2 and V_1H_2 coincidences in both collection modes are symmetric under exchange of λ_1 and λ_2 , which simply reflects the fact that the two collection modes are chosen to exhibit a mirror symmetry with respect to a plane containing the optical axis of the crystal and the pump direction.

To quantify the spectral distributions, we use a two-dimensional Gaussian as a model:

$$g(\lambda_1, \lambda_2) \propto e^{-\frac{1}{2} \left[\frac{(\lambda_1 - \bar{\lambda}_1)^2}{\sigma_1^2} + \frac{(\lambda_2 - \bar{\lambda}_2)^2}{\sigma_2^2} + \frac{(\lambda_1 - \bar{\lambda}_1)(\lambda_2 - \bar{\lambda}_2)}{\sigma_{12}} \right]} \quad (3)$$

Therein, we obtain from a fit to the H_1V_2 joint spectrum displayed in the upper panel of Fig. 2 a central wavelength of $\bar{\lambda}_1 = 779.77 \pm 0.01$ nm for the extraordinary, and $\bar{\lambda}_2 = 779.10 \pm 0.01$ nm for the ordinary distribution, reflecting an alignment close to the degeneracy point. For the quantities governing the shape of the distribution, we obtain $\sigma_1 = 1.265 \pm 0.003$ nm, $\sigma_2 = 1.853 \pm 0.005$ nm for the standard deviations, and $\sigma_{12} = 1.509 \pm 0.009$ nm² as a measure of the covariance of the two wavelengths.

Each distribution is *not* symmetric with respect to exchange in the two wavelengths. This will lead to spectral regions where the balance of the two decay paths necessary to observe a maximally entangled polarization state of the form Eq. (2) is not met. Another consequence of the asymmetry is a different width of the marginal distributions for both ordinary and extraordinary polarization. For the assumed two-dimensional Gaussian distribution,

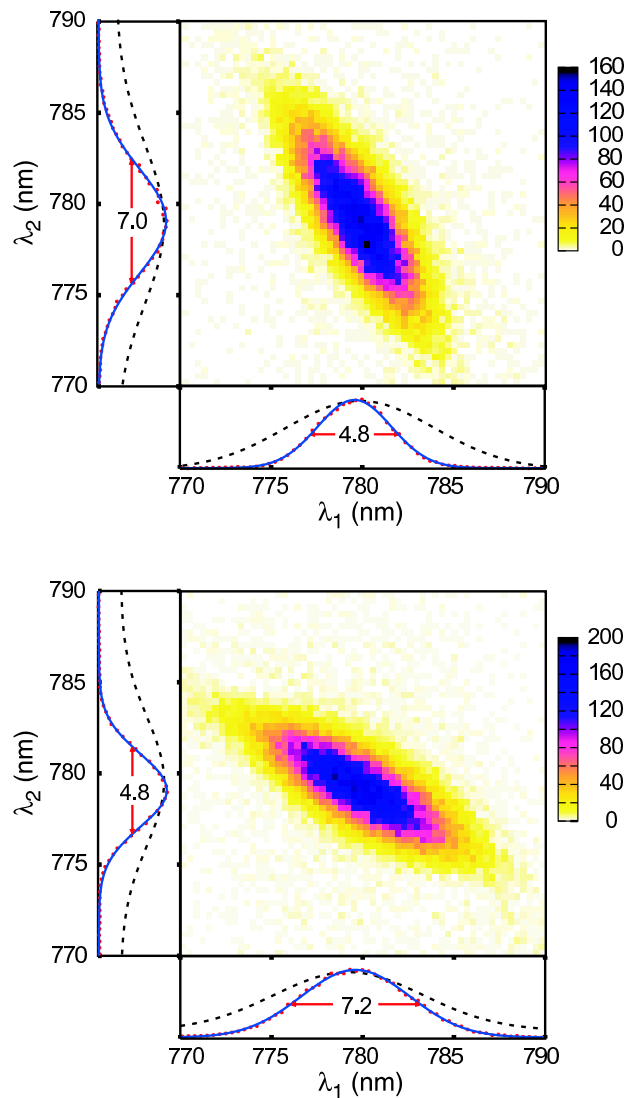


FIG. 2: The joint spectra of coincidence counts for H_1V_2 polarizations (upper panel) and V_1H_2 (lower panel) polarization are different. Exchange of the λ_1 and λ_2 axis maps one onto the other. These joint spectra show the covariance between λ_1 and λ_2 , which decreases with the broadening of the pump light. Different widths between the marginal (solid trace) and the single photon event spectrum (dotted trace), as well as differences between ordinary and extraordinary polarization are apparent.

the marginals exhibit a width (FWHM) of

$$\Delta\lambda_{m1,2} = 2\sqrt{2 \log 2} \left(\frac{1}{\sigma_{1,2}^2} - \frac{\sigma_{2,1}^2}{4\sigma_{12}^2} \right)^{-1/2} \quad (4)$$

or $\Delta\lambda_{m1} = 4.83 \pm 0.02$ nm for the extraordinary polarization and $\Delta\lambda_{m2} = 6.97 \pm 0.05$ nm for the ordinary polarization for the H_1V_2 combination and similar results for the V_1H_2 combination. Since the marginal distributions represent a conditional spectrum of having seen a photon

at any wavelength in the other arm, this indicates that the collection bandwidth for both polarizations is slightly different due to the dispersion relations in the crystal. A collection optics with a fixed capture angle will therefore have an imbalanced collection efficiency for both polarizations, limiting the overall collection efficiency of type-II SPDC for generating entangled photon pairs.

Compared to the widths of the distributions of single photon events (dashed lines in the marginal distributions of Fig. 2, $\Delta\lambda_H = 8.3$ nm, $\Delta\lambda_V = 9.9$ nm) the widths of the marginal spectra are also considerably smaller (contrary to a statement in [23]). This is not observed in a cw pumped source, but can be understood as a consequence of a finite pump bandwidth and the dispersion relations for the phase matching conditions Eq. (1). Again, this difference in spectral width is an indicator for a reduced collection efficiency, as not every photon in one collection fiber will find its twin from the down-conversion process in the other collection fiber, in general in agreement with the reduced pair/single ratio observed in femtosecond-pumped SPDC sources.

To understand the effect of the spectral imbalance between the different polarization components on the polarization entanglement, we mapped out joint spectra for polarizations in a basis complementary to the natural polarizations of the crystal, or the $\pm 45^\circ$ linear polarizations in our case. The results are shown in Fig. 3, where the upper panel corresponds to polarization anti-correlations ($\alpha_1 = -\alpha_2 = 45^\circ$), and the lower panel to polarization correlations ($\alpha_1 = \alpha_2 = 45^\circ$). The integration time per wavelength pair was 30 s for the anti-correlations, and 60 s for the correlations. For the latter case, the mapping was done in a sequence of four interlaced grids. A drift of the system over the data acquisition period thus lead to a modulation of the coincidence counts at twice the final sampling spacing. Since the phase δ between the two decay paths was adjusted to prepare photon pairs in a $|\Psi^-\rangle$ state, a relatively large overall count rate is observed for the polarization anti-correlations. As expected, a maximal coincidence count rate occurs at the degeneracy point and is progressively reduced away from it, following the spectral distribution of the overlap of the H_1V_2 and V_1H_2 contributions from Fig. 2. An interesting pattern is revealed for the anti-correlations: while there are no coincidences at the degenerate wavelength point, four regions with non-vanishing coincidence events are observed. These regions correspond to an imbalance in the decay path distribution, and will destroy the perfect polarization anti-correlations in the $\pm 45^\circ$ basis in an experiment where the wavelengths of both photons are ignored.

V. SPECTRALLY RESOLVED ENTANGLEMENT CHARACTERIZATION

The presence of residual polarization correlations at particular wavelength regions could be both due to the

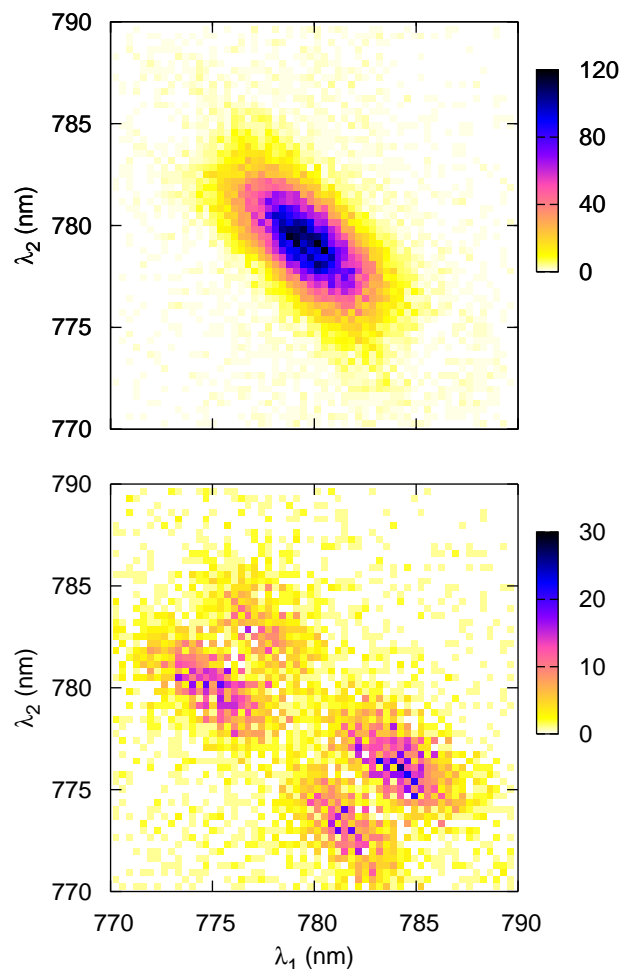


FIG. 3: A joint spectrum of coincidences measured for a $+45^\circ/-45^\circ$ polarization combination (upper panel) reveals a pattern with the maximum coincidence rate at the degenerate wavelengths for a source adjusted to observe singlet Bell states $|\Psi^-\rangle$. The joint spectrum measured for a $+45^\circ/+45^\circ$ polarization combination (lower panel) exhibits four regions of higher count rate. These regions correspond to area with an imbalance of a and b . At the position of the degenerate wavelengths in the center, the coincidence rate is close to zero.

imbalance of both components, or due to a partially incoherent superposition between them as a consequence of entanglement with other degrees of freedom. We therefore carried out polarization correlation measurements on a larger set of relative analyzer angles for the different wavelength regions. Again we fixed the analyzer orientation for one mode to $\alpha_1 = +45^\circ$, and varied the orientation for the other analyzer.

The result of (normalized) coincidence counts obtained during 60 seconds per polarizer setting for three representative regions in the spectral map are shown in Fig. 4. Trace A corresponds to a region with an excess of the $|V\rangle_1|H\rangle_2$ component, trace B to a region with a predominance of the $|H\rangle_1|V\rangle_2$ contribution, and trace C to the

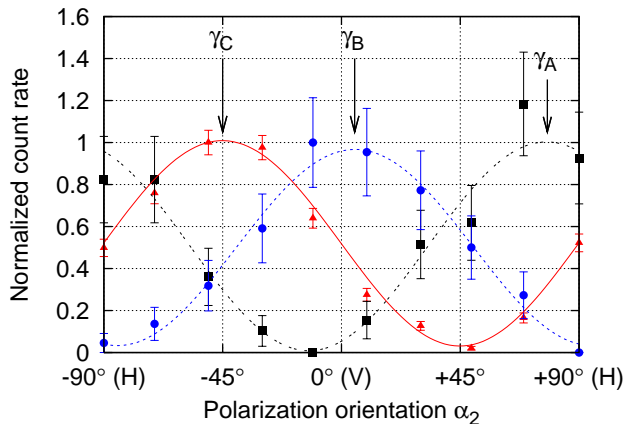


FIG. 4: Polarization correlations at three different wavelength pairs where one photon is projected onto $+45^\circ$ polarization. The maximum of coincidences ranges from -45° polarization for a maximally entangled singlet Bell state (C), to the horizontal (A) or vertical (B) polarization.

degeneracy point. The normalization was carried out for better reading of the diagram due to the varying number of coincidences in the different spectral regions. It is apparent that at all points, the sinusoidal modulation of the polarization correlations shows a high visibility, while the angle α_2 for the maximum depends strongly on the spectral position. For the following, we denote this maximum angle by γ . For the three samples shown in Fig. 4, we obtained visibilities of $V_A = 98 \pm 12\%$, $V_B = 93 \pm 6\%$, and $V_C = 98 \pm 5\%$ from a sinusoidal fit, all compatible with 100% within the measurement accuracy, and rotations of $\gamma_A = 79.0 \pm 1.6^\circ$, $\gamma_B = 5.0 \pm 0.8^\circ$, and $\gamma_C = -45 \pm 0.6^\circ$, respectively.

A map of both the visibility $V(\lambda_1, \lambda_2)$ and the angle $\gamma(\lambda_1, \lambda_2)$ for analyzer 1 at $\alpha_1 = +45^\circ$ is displayed in Fig. 5 (upper panel) at wavelength pairs with a large enough coincidence count rate to extract visibilities with an uncertainty below 11%. This map confirms the high visibility of the polarization correlations for all wavelengths. While quoting a high visibility V_{45} of polarization correlations with one of the polarizers oriented at 45° is in itself not enough to make a statement about the entanglement of photon pairs in general, the additional information that only two decay processes in SPDC are allowed reduces the discussion to an analysis of the coherence between these decay processes. This is covered completely by the visibility measurement in the $+45^\circ / -45^\circ$ basis; hence its wide usage as a quick indicator for the entanglement quality of a photon pair source from SPDC.

For our case, V_{45} is compatible with 100% within errors at all locations, suggesting that the superposition between the two decay components is indeed coherent, and that the polarization state at each wavelength pair is pure. The state can therefore be written as a superposition of the two decay process contributions,

$$|\Psi(\lambda_1, \lambda_2)\rangle = a |H\rangle_1 |V\rangle_2 + b e^{i\delta} |V\rangle_1 |H\rangle_2 \quad (5)$$

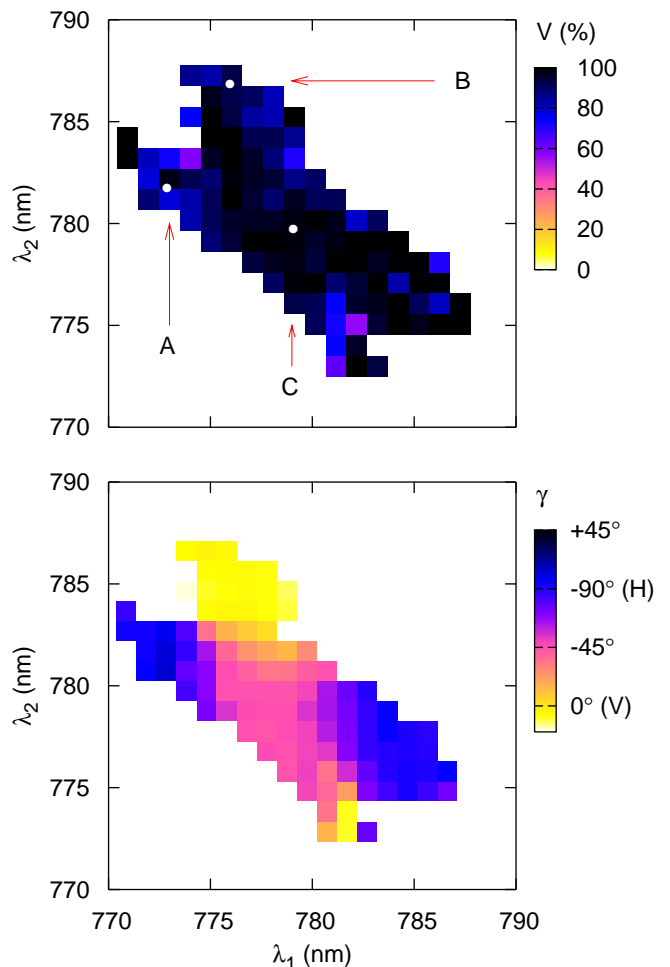


FIG. 5: Map of the visibility V_{45} of polarization correlations for different sets of wavelengths (upper panel). The high visibility for all areas with significant pair contributions reveals that the polarization state is pure if the wavelength is measured. Points A, B and C correspond to the three detailed visibility measurements in Fig. 4. The lower panel indicates the angle γ for the maximal count rates, ranging from -45° polarization for the singlet Bell state at (C) in the center towards horizontal polarization (A) for dominating $|V\rangle_1 |H\rangle_2$ contributions or vertical polarization (B) for prevailing $|H\rangle_1 |V\rangle_2$ contributions.

with two wavelength-dependent probability amplitudes $a(\lambda_1, \lambda_2)$ and $b(\lambda_1, \lambda_2)$. The fact that a perfect visibility is observed with linear polarizations at 45° implies that there is no complex phase factor between the amplitudes a and b . For imbalanced amplitudes a and b , the corresponding superposition state is still pure, but not maximally entangled anymore. The angle γ depends now only on the ratio between real-valued probability amplitudes a and b :

$$\gamma = -\arctan \frac{b}{a} \quad (6)$$

It is worth noting that the high symmetry of the imbalanced states in the frequency map allows for com-

compensation techniques [17] that combine different spectral components so that they do not reveal information about the polarization. If this combination is performed appropriately, the spectral degree of freedom is factored out of the description of the state (much like the timing compensation performed by the compensation crystals) and no longer degrades the polarization entanglement.

Knowing that the polarization state at each wavelength pair is pure but not necessarily maximally entangled, we can use the spectral map of the $|H\rangle_1|V\rangle_2$ and $|V\rangle_1|H\rangle_2$ contributions displayed in Fig. 2 to extract a local measure for the entanglement quality in the polarization degrees of freedom: A commonly used quantity for this purpose is the entropy of entanglement S . For a local polarization state given by Eq. (5), the entanglement entropy is given by [24]

$$S(\lambda_1, \lambda_2) = -a^2 \log_2(a^2) - b^2 \log_2(b^2) \quad (7)$$

The spectral distribution of the probability amplitudes can be chosen as

$$a(\lambda_1, \lambda_2) = \sqrt{\frac{g(\lambda_1, \lambda_2)}{g(\lambda_1, \lambda_2) + g(\lambda_2, \lambda_1)}} \quad (8)$$

$$b(\lambda_1, \lambda_2) = \sqrt{1 - a(\lambda_1, \lambda_2)^2}$$

with a spectral distribution $g(\lambda_1, \lambda_2)$ of photon pairs. Using a model expression according to Eq. (3) for g , we obtain an expected spectral entanglement entropy distribution shown in the upper panel of Fig. 6. Along the two diagonals, the entropy is maximal, indicating maximally entangled states due to the balanced contributions from both decay paths. The lower panel of this figure shows the entanglement entropy S extracted from the distributions of both decay components obtained from measurements presented in Fig. 2. The entropy is only computed at locations where the overall count rate allowed for reasonable error bars. Again, the distribution of maximally entangled states in the spectral map is clearly revealed.

VI. DEPENDENCE OF ENTANGLEMENT QUALITY ON SPECTRAL FILTERING

When the wavelengths of a photon pair are ignored and only polarization correlations are probed, integrating all spectral contributions with their varying γ results in a reduced overall visibility V_{45} even if the individual wavelength components exhibit a high visibility. In practice this results in a mixed state with lower entanglement quality; to remedy this, spectral filtering, either in the form of interference filters [4] or careful engineering of the collection bandwidth can be used [21]. These filters spectrally limit the λ_1, λ_2 of the down-converted photon pairs to a smaller region, thus reducing contributions with γ deviating from the value in the degeneracy point. Consequently, there is a tradeoff between the coincidence rate and the measured visibility. For very narrow spectral filters entanglement quality will be high but count

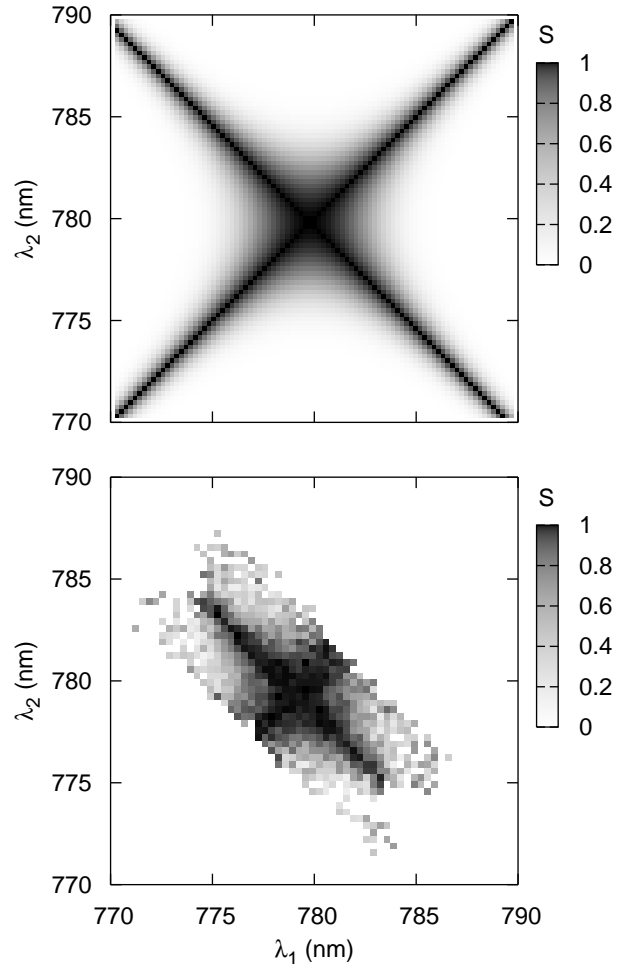


FIG. 6: Entanglement quality. The upper panel illustrates the entanglement entropy S as a function of both wavelengths λ_1, λ_2 for a model distribution of non-overlapping contributions for $|H\rangle_1|V\rangle_2$ and $|V\rangle_1|H\rangle_2$ decay paths in SPDC according to Eq. (3). The lower panel shows $S(\lambda_1, \lambda_2)$ obtained from experimental polarization correlations in the $+45^\circ/-45^\circ$ basis of Fig. 2. The entanglement is maximal at positions with balanced contributions for both decay paths.

rates low; as the filter bandwidth is increased, count rates increase but the entanglement quality is reduced. The polarization correlations underlying the visibility map, Fig. 5 (upper panel), offer a way to determine the optimal filtering scheme given some entanglement-based figure of merit.

For a virtual experiment with filter transmissions $f_{1,2}(\lambda_{1,2})$, the coincidence rate distribution $C(\alpha_2)$ necessary to determine the polarization correlation visibility for $\alpha_1 = 45^\circ$ can be obtained by weighting the contributions $c(\lambda_1, \lambda_2, \alpha_2)$ from the different wavelength pairs we

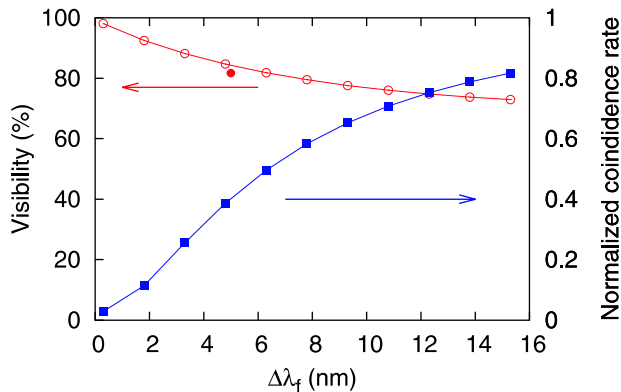


FIG. 7: Visibility V_{45} (open circles) and normalized coincidence rates (filled squares) as a function of fixed filter bandwidth $\Delta\lambda_f$. The values were obtained by virtual filtering using the spectral map of visibility measurements leading to Fig. 5. The experimental point (filled circle) corresponds to a real filter with $\Delta\lambda_f = 5$ nm, resulting in $V_{45} = 81.7\%$. Our result is consistent with predictions in [25].

already measured to generate the visibility map in Fig. 5:

$$C(\alpha_2) = \sum_{\lambda_1, \lambda_2} c(\lambda_1, \lambda_2, \alpha_2) f_1(\lambda_1) f_2(\lambda_2) \quad (9)$$

The visibility V_{45} itself is then extracted from a sinusoidal fit of $C(\alpha_2)$.

Typical filter transmission functions of narrow-band interference filters can be described by a Lorentzian profile and are characterized by their central wavelength λ_f and bandwidth $\Delta\lambda_f$ (FWHM). The resulting integral visibility V_{45} for filters with the same transmission profiles $f_1(\lambda) = f_2(\lambda)$ centered at the degeneracy wavelength in both arms is shown in Fig. 7 (open circles). As expected, the visibility drops with an increasing bandwidth $\Delta\lambda_f$ of the filters, in agreement with the theoretical predictions in [25]. We also include a normalized coincidence count rate (filled squares) extracted out of the weighted virtual counts $C(\alpha)$ to illustrate the loss of pairs at narrow bandwidths.

As a check of consistency, we can compare the expected visibility from virtual filtering with a direct measurement of the V_{45} for a filter with $\Delta\lambda_f = 5$ nm. From Fig. 7 we expect $V_{45} = 84.5\%$ while in a direct measurement we observe $V_{45} = 81.7\%$. This difference is

due to the fact that for SPDC in femtosecond regime, higher order contributions in form of four-photon states become significant. When performing two-photon measurements, this four-photon contribution will manifest as photon pairs which are uncorrelated in polarization, thus resulting in a lower visibility V_{45} . We estimated the coincidence rate from this contribution by looking at pair coincidences between consecutive pulses. Correction for this four-photon contributions leads to a two-photon visibility of $\tilde{V}_{45} = 85.8 \pm 0.3\%$, in reasonable agreement with the result from virtual filtering.

VII. CONCLUSIONS

In this paper, we reported on spectrally resolved polarization correlation experiments produced by SPDC in a femtosecond regime. The objective was to clarify the relation between entanglement quality and spectral distinguishability of the decay paths contributing to the entangled state.

We found that the two decay paths are distinguishable in their spectral properties and that this information leakage is enough to explain all the entanglement degradation in polarization. Detailed measurements revealed that, if the spectral degree of freedom is taken into account, the detected state is always pure, though not maximally entangled. As a consequence, no additional degree of freedom is necessary to usefully describe the state produced in SPDC in traditional entangled photon experiments.

Using the spectrally resolved polarization correlations we constructed a map of the entanglement entropy over the joint spectrum of the down-converted pairs, showing that the entanglement is maximum at those positions which have equal contributions from the two decay paths.

The presented virtual filtering technique could be useful in finding the optimal choice of filters given a particular entanglement figure-of-merit to be maximized in combination with a count rate.

Acknowledgment

This work was supported by the Quantum Information Technology (QIT) project of A*STAR. We like to acknowledge helpful discussions with Piotr Kolenerski from Torun University.

-
- [1] D. Bouwmeester, A. Ekert, and A. Zeilinger, *The physics of quantum information* (Springer, 2001).
 - [2] D. C. Burnham and D. L. Weinberg, *Physical Review Letters* **25**, 84 (1970).
 - [3] D. N. Klyshko, *Photons and Nonlinear Optics* (Gordon and Breach Science Publishers, New York, 1989).
 - [4] P. G. Kwiat, K. Matile, H. Weinfurter, A. Zeilinger, A. V.

- Sergienko, and Y. Shih, *Phys. Rev. Lett.* **75**, 4337 (1995).
- [5] T. Jennewein, C. Simon, G. Weihs, H. Weinfurter, and A. Zeilinger, *Phys. Rev. Lett.* **84**, 4729 (2000).
- [6] J. Brendel, E. Mohler, and W. Martienssen, *Europhys. Lett.* **20**, 575 (1992).
- [7] P. G. Kwiat, E. Waks, A. G. White, I. Appelbaum, and P. H. Eberhard, *Physical Review A* **60**, R773 (1999).

- [8] D. Bouwmeester, J. Pan, K. Mattle, M. Daniell, M. E. H. Weinfurter, and A. Zeilinger, *Nature* **390**, 575 (1997).
- [9] A. Lamas-Linares, J. C. Howell, C. Simon, and D. Bouwmeester, *Science* **296**, 712 (2002).
- [10] M. Eibl, S. Gaertner, M. Bourennane, C. Kurtsiefer, M. Zukowski, and H. Weinfurter, *Physical Review Letters* **90**, 200403 (2003).
- [11] M. Zukowski, A. Zeilinger, and H. Weinfurter, *Ann. NY Acad. Sci.* **755**, 91 (1995).
- [12] W. P. Grice, R. Erdmann, I. A. Walmsley, and D. Branning, *Physical Review A* **57**, R2289 (1998).
- [13] F. A. Bovino, P. Varisco, A. M. Colla, G. Castagnoli, G. D. Giuseppe, and A. V. Sergienko, *Optics Communications* **227**, 343 (2003).
- [14] D. Branning, W. P. Grice, R. Erdmann, and I. A. Walmsley, *Physical Review Letters* **83**, 955 (1999).
- [15] R. Erdmann, D. Branning, W. Grice, and I. A. Walmsley, *Physical Review A* **62**, 053810 (2000).
- [16] W. P. Grice, A. B. U'Ren, and I. A. Walmsley, *Physical Review A* **64**, 063815 (2001).
- [17] Y.-H. Kim and W. P. Grice *J. Mod. Opt.* **49**, 2309 (2002).
- [18] J. F. Hodelin, G. Khoury, and D. Bouwmeester, *Phys. Rev. A* **74**, 013802 (2006).
- [19] J.-W. Pan, D. Bouwmeester, H. Weinfurter, and A. Zeilinger, *Phys. Rev. Lett.* **80**, 3891 (1998).
- [20] A. Aspect, P. Grangier, and G. Roger, *Physical Review Letters* **49**, 91 (1982).
- [21] C. Kurtsiefer, M. Oberparleiter, and H. Weinfurter, *Physical Review A* **64**, 023802 (2001).
- [22] A. Ling, K. P. Soh, A. Lamas-Linares, and C. Kurtsiefer, *Laser Physics* **16**, 1140 (2006).
- [23] Y.-H. H. Kim and W. P. Grice, *Optics Letters* **30**, 908 (2005).
- [24] C. H. Bennett, H. J. Bernstein, S. Popescu, and B. Schumacher, *Phys. Rev. A* **53**, 2046 (1996).
- [25] W. P. Grice and I. A. Walmsley, *Physical Review A* **56**, 1627 (1997).